IOP Conference Series: Materials Science and Engineering

PAPER • OPEN ACCESS

Optimization of friction stir welding parameters using response surface methodology

To cite this article: I Sabry *et al* 2020 *IOP Conf. Ser.: Mater. Sci. Eng.* **973** 012017

IOP Conf. Series: Materials Science and Engineering **973** (2020) 012017 doi:10.1088/1757-899X/973/1/012017

Optimization of friction stir welding parameters using response surface methodology

I Sabry[1], N Gadallah[1] and M Abu-Okail[1]
[1] Manufacturing Engineering Department, Modern Academy for Engineering and Technology, Cairo, Egypt
ibrahim_sabry@f-eng.tanta.edu.eg

Abstract. The aim of this article is to create a new technique for predicting discontinuity formation, its place and magnitude during aluminium alloy (AA6061) friction stir welding (FSW). The effectiveness of the technique was demonstrated using visual inspection, hardness and tensile test of the friction stir welded joints. The measured current was analysed through power calculations. In each of the FSW stages, the energy consumption is significantly varied, clearly distinguishing the penetration of the tool, its revolution, its traverse movement and its metal removal rate. The findings of tracking the energy consumption indicate that using power consumption means the significance of weld quality. FSW has been carried out based on two factors - two levels. Response surface methodology (RSM) is employed to develop a mathematical model. Analysis of variance (ANOVA) technique checks the adequacy of the developed mathematical model, which is used effectively at 95% confidence level. In contrast, tensile and hardness tests also showed that welds at high power usage failed continuously within the welding area, due to reduced welding temperature and absence of penetration in the welding zone.

1. Introduction

Friction stir welding, a comparatively fresh joining method invented at the Welding Institute in 1991, is a method that falls into a solid-state joining one that allows a plastic deformation and physical intermixing of two or more materials [1]. A friction stir welding process scheme is shown in figure1. A non-consumable rotating tool composed of a shoulder and a pin plunging into the workpieces during friction stir welding so that the shoulder and the workpieces are in contact.

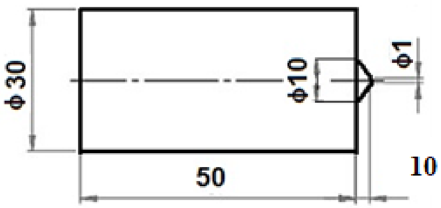

Figure 1. Conical friction stir welding tool

Due to an elevated heat field arising from the mixture of high tool-workpiece interface and friction forces, a plastic deformation under the rotating tool is produced. The instrument passes along the joint interface and joins the neighbouring workpieces as the instrument leaves the processing area. One of the main approaches to define critical surveillance and forecast characteristics has concentrated on frequency analysis of measured output signals [2]. The main reason behind this is that discontinuity formation results from the uneven material flow that has been plasticized. Evidence indicates that the plasticized material around the tool probe flows into a cavity created at the probe's trailing edge as the tool rotates and moves. The plasticized material flow is extremely regular in relation to the tool rotation frequency under correct welding conditions [3].

In case of defective welds, the cavity is partially filled at the tool's rotational frequency, and the material flow is not purely periodic. The ability to detect and monitor the formation of voids is to analyse the output signals. These measured signals include acoustic emission, dipping force, vertical and traverse forces, spindle or feed engine current, and surface pictures. With a mixture of discrete wavelet conversion, Chen et al.[4] used acoustic emission signals. Based on the research conducted by Chen et al, Sundararajan et al. [5] diverse welding parameters (welding velocity, spindle speed and dip depth) are used to explore the impact of process parameters on changes in acoustic emission signals. The option of automatically identifying gap-induced failures provided by Fleming et al. [6], with a Fast Fourier Transform, the plunge forces were gathered and processed. The statistical analysis showed that the frequency spectrum of measured dip force could be a main characteristic in identifying defective welds by discovering discriminating features.

Kumar and Kumari et al. [7] evaluated surface defect correlation with abrupt modifications in plunge force. In order to locate the faulty surface area, statistical characteristics such as variance and square of detail coefficient mistakes obtained from constant and discrete wavelet transformations were introduced. Das et al. [8] obtained spindle, feed motor currents, and extracted decomposed characteristics from the signals using wavelet conversion. The characteristics along with process parameters (welding velocity, spindle speed and the tool's shoulder diameter) were supplied to artificial neural network algorithms to predict ultimate tensile strength of the workpieces and weld strength. Attempts to classify welds as defect-free or faulty using different statistical techniques and approaches to machine learning. Instant frequency and stage data were obtained from the measured plunge force through the established technique. Sectioning the welds at random places verified the inner voids. The writers indicated that both characteristics (instant frequency and phase) could describe the existence of defects in the welded samples effectively.

Boldsikhan et al. [9] explored the use of a discrete Fourier transformation and a method of machine learning to separate faulty welds from defect-free welds. For classification, the decomposed reduced frequency sections of the vertical and traverse force signals frequency spectrum were fed into the neural network. The data set tested showed a classification precision of roughly 95%..Shrivastava et al. [10] introduced computerized tomography (i.e. 3D X-ray imagery) to evaluate the complete volumetric size of sub-surface voids generated in the friction stir welded specimens. Specimen with variable error sizes (formed by variable input parameters such as spindle velocity and weld velocity) were evaluated using the frequency content (via quick Fourier Transform) of the force signal measured in the weld travel direction and using a statistical method. Their works showed a nice correlation between the welding force frequency content and the occurrence and voids size.

The power usage of 6061-T6 aluminium friction stir welding and gas metal arc welding was earlier compared [11] using a single parameter situation (welding velocity: 400 mm/min, spindle velocity: 1100 rpm and steel backing plate) where general power consumption in friction stir welding was discovered to be 40% lower than gas arc welding in this specific welding situation. Hence, the FSW process parameters, rotation speed and travels speed effect the power consumption, current, Cooling rate, ultimate tensile strength, yield strength, and percentage of elongation in FSW joints. There is a gap between predicting power consumption, current, Cooling rate, ultimate tensile strength, yield strength, and percentage of elongation for different parameters and for various materials. This gap could be filled by developing an RSM based model for the FSW process. In this work, an attempt was made to develop a straightforward RSM for the prediction of weld strength and hardness, within the range of the process parameters, which could provide a perfect joint through utilize FSW.

2. Experimental work

2.1 Material and Experimental Setup:

The AA6061 aluminum alloy plates (workpieces) were milled to nominal dimensions of 10 x 75 x 300 mm.

Table 1.chemical composition (wt%) of AA 6061 (ASTM D3039).

Alloy	6061
Si	0.6
Fe	0.7
Cu	0.28
Mn	0.15
Mg	0.2
Ti	0.15
Cr	0.2
Zn	0.25

Table 2. Mechanical Properties of AA 6061

Description	6061
σy MPa	85
σu1MPa	122
E1 %	16
VHD	62

The plates are mounted in a rigidly developed fixture. During the welding process, the tool is fed with 2mm penetration depth. The plate were welded using friction stir welding equipment Egypt (EG) FSW. The spindle current consumed for the welding process is acquired for every weld. The rotational speed and feed rate were fixed at 1000, 1400 and 1800 rpm and 10, 16 and 31.5 mm/s respectively after several welding trials. The tool tilt was 2˚. The geometrical dimensions of the conical friction stir welding tool that is used for the experimentation are shown in figure 1. Table 3 shows the parameters used for the welding of AA 6061 plate. The Scheme of the overall approach used in monitoring and controlling friction stir welding is shown in figure 2 (a) and The Scheme of the overall approach used in monitoring and controlling friction stir welding is shown in figure 2 (b). The scheme of the definitions of cooling rate and temperature gradient is shown in figure 3.

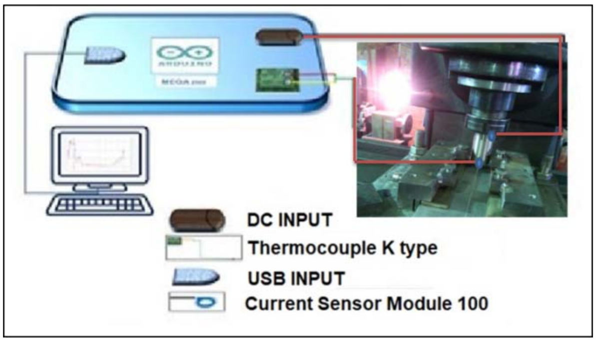

Figure2.Scheme of friction weld overall approach used in monitoring and controlling friction stir welding

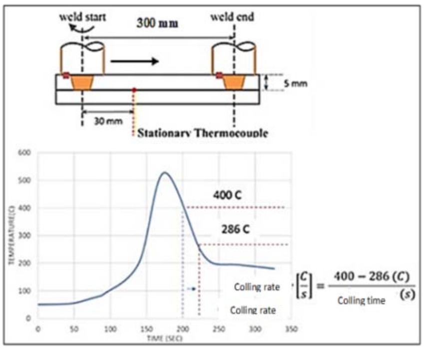

Figure3. Definitions of cooling rate and temperature gradient.

IOP Conf. Series: Materials Science and Engineering **973** (2020) 012017 doi:10.1088/1757-899X/973/1/012017

2.2 FSW process variables

Based on preliminary trials and previous studies, the independent process parameters affecting the power consumption, current, Cooling rate, temperature, ultimate tensile strength, and percentage of elongation were identified as rotation speed (N), and travel speed (S). Table 3 shows the friction stir welding parameters.

Table 3. Parameters for friction stir welding of Al 6061

Parameter	Value
Tool rotation [rpm]	1000,1400,1800
Tool feed rate [mm/min]	10,16,31.5

Trial runs proceeded to find the upper and lower limit of process parameters for AA 6061 by changing one parameter only at each time. A parameter range was tuned in such a way that the final welded joint has no defects recognized by visual screening. The upper limit of a factor was coded as 1 and lower limit as −1. The intermediate coded values were calculated using equation(1).

$$X_i = 2X - \frac{X_{max} + X_{min}}{X_{max} - X_{min}} \qquad (1)$$

where X_i, X,X_{max} and X_{min} are the wished-for coded value, the variable value, the lower limit of the variable and the upper limit of the variable respectively [14]. Table 4 specify the considered process parameters with their limits, units and notations.

Table 4. Parameters Process and Their Levels in FSW

Process Parameters	Unit	Levels		
		-1	0	1
Tool rotation[rpm]	N	1000	1400	1800
Tool feed rate[mm/min]	S	10	16	31.5

Specimens of required size were cut from the welded plate to execute out metallurgical studies as explained in figure 4.a. Figure 4.b represents the sample of FSW welded at 10 mm/min and 1000 rpm.

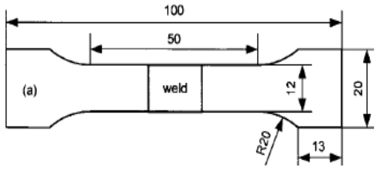

Figure4(a).Tensile test sample geometry.**Figure4(b)**. A sample of FSW welded.

3. Results and discussion

The tensile test samples were according to ASTM D3039. The ultimate tensile strength of the FSW joints were measured through computerized universal testing machine. For each welded joint, four specimens were prepared and tested. Table 5 presents the average values of the results acquired from FSW experimental values.

The experiment was based on two factors with three levels of full factorial experimental design. As prescribed in the Experimental design matrix night joints were carried out by considering three levels of a process parameter, namely tool rotational speed and travels speed as given in the Table 2. It is to be further noted that the experiments were conducted with a constant tool rotational speed and travels speed.

Table 5.Experimental design matrix and results

Trial no.	Coded value		Real value		Experimental work					
	N	S	Tool speed (rpm)	Travels speed (mm/min)	Temperature	Cooling rate	Tensile strength	Power process	Elongation	Current consumption
1	1	1	1000	10	480	65	235	2500	0.68	4.8
2	1	2	1000	16	471	29	220	1500	0.60	4.5
3	1	3	1000	31.5	450	11	210	1450	0.55	4.1
4	2	1	1400	10	500	55	245	2700	0.65	6.5
5	2	2	1400	16	485	25	230	1700	0.612	6.2
6	2	3	1400	31.5	465	15	212	1500	0.6	6
7	3	1	1800	10	550	70	250	3000	0.70	8
8	3	2	1800	16	510	22	237	1900	0.6256	7.8
9	3	3	1800	31.5	500	19	215	1600	0.63	7.3

3.1 Mathematical Model:

Ultimate tensile strength, hardness and surfaces roughness of the FSW joints is function of rotation speed, travel speed and axial force, and it can be expressed as in Eq. 2.

$$Y = f(N,S) \tag{2}$$

where Y is the response, N is the rotation speed and S is the travel speed. For the three factors, the chosen polynomial could be expressed as in equation (3).

$$Y = \beta_0 + \beta_1 N + \beta_2 S + \beta_{11} N^2 + \beta_{22} S^2 + \beta_{12} NS \tag{3}$$

where β_0 is the free term of the regression equation, β_1, and β_2 are the linear terms, the coefficients β_{11}, and β_{22} are quadratic terms, the coefficients β_{12} are the interaction terms. The values of the coefficient of the polynomial are calculated by regression analysis with the help of following equations [3]:

$$\beta_0 = 0.1663 \sum(\mathrm{Y}) - 0.0568 \sum\sum(\mathrm{X_{ii}Y}) \tag{4}$$

$$\beta_j = 0.0732\,(\mathrm{X_iY}) \tag{5}$$

$$\beta_j = 0.0625 \sum(\mathrm{X_{ii}Y}) + 0.00689 \sum\sum(\mathrm{X_{ii}Y}) - 0.0568 \sum(\mathrm{Y}) \tag{6}$$

$$\beta_{ij} = 0.1250 \sum(\mathrm{X_{ij}Y}) \tag{7}$$

where i ; j = 1, 2, 3 and i< j

DESIGN EXPERT 8.0.4 software package has been used to estimate the values of those coefficients for different responses and the results are presented in Table 6.

Table 6 Calculated regression coefficients of mathematical model

Regression factor	Temperature	Cooling rate	Tensile strength	Power	Elongation	current
$\boldsymbol{\beta_0}$	568.6	225.8	224.2	4781.	0.9980	-0.4065
$\boldsymbol{\beta_1}$	-0.09721	-0.08063	0.04845	0.3893	-0.0001976	0.006697
$\boldsymbol{\beta_2}$	-5.473	-13.72	-3.056	-337.8	-0.02725	-0.06733
$\boldsymbol{\beta_{11}}$	6.354E-005	2.708E-005	-7.292E-006	0.0001563	6.417E-008	-9.375E-007
$\boldsymbol{\beta_{22}}$	0.1144	0.2636	0.06110	7.460	0.0004395	0.0009669
$\boldsymbol{\beta_{12}}$	-0.0007541	0.0003808	-0.0006584	-0.02031	3.668E-006	-1.608E-006

IOP Conf. Series: Materials Science and Engineering **973** (2020) 012017 doi:10.1088/1757-899X/973/1/012017

3.2 Checking the adequacy of the developed models using ANOVA

The sufficiency of the advanced models employ the analysis of variance technique (ANOVA). The contribution percentage (p) signalizes the linear square and interaction process parameters with the response functions. These (p) values are employed to identify the significant parameters on the response functions [12]. Table 6 demonstrates the results for tensile strength model of the ANOVA. The model F-value of 17.25, 19.98, 99.63, 2011.3, 9.58 and 370.33 for temperature, cooling rate, tensile strength power process, elongation%, current consumptions implies the model is significant. There is only a 0.01% chance that a model F-value could occur due to noise. Value NS is significant model terms. Values better than 0 1 indicate that the model terms are not significant. The coefficient of determination R2 values gives the goodness of fitness of the model. The determined values of the developed model are presented in Table 7.

Table 7. Coefficient of determination values for temperature, cooling rate, tensile strength, elongation, current and power process

	F-value	R^2	*Adusted* R^2	*Predicted* R^2	*Adequate Precision*
Temperature model	17.25	0.9664	0.9104	0.6648	12.58
Cooling rate model	19.98	0.9709	0.9223	0.7023	10.35
Tensile strength model	99.63	0.9940	0.9840	0.9274	28.10
Elongation model	9.58	0.9409	0.8425	0.3107	8.882
Current model	370.33	0.9984	0.9957	0.9753	50.40
Power processes model	2011.3	0.9997	0.9992	0.9981	113.1

3.3 Effect of FSW process parameters

The tensile strength, elongation%, current consumption, power, cooling rate and temperature of FSW welded aluminium alloy 6061 were predicted by the mathematical models using the experimental observations presented in figure 5, showing the general trends between predicted and experimental results. The results of the ANOVA are given in table 6. The validity of regression models developed is further tested by drawing scatter diagrams presented in Fig.5 (a-f). The observed values and predicted values of the responses are scattered close to the 45° line, indicating an almost perfect fit of the developed empirical models [13].

Surface plot for temperature due to interaction effect of the travels and rotational speed is shown in figure 6 (a). The increase in temperature is significant at larger rotation speed while insignificant increase in temperature at low travels speed is observed. Surface plot for cooling rate due to interaction effect of the rotational and travels speed is shown in figure 5 (b). Figure 5 (c) shows the interaction effect of rotational and travels speed on the tensile strength. Figure 5 (c) shows surface plot for tensile strength due to interaction effect of the travels and rotational speed. The increase in tensile strength is significant at larger rotational speed while insignificant increase in tensile strength at low travels speed is observed. Surface plot for elongation percentage due to interaction effect of rotational and travels speed is shown in figure 6 (e). Surface plot for power process due to the interaction effect of the rotational and travels speed is shown in figure6 (d). Figure 6 (f) shows the increasing trend of current consumption at higher rotational and travels speeds as compared to lower rotational speed. Surface plot for current consumption due to interaction effect of the rotational and travels speed is shown in figure6 (f).

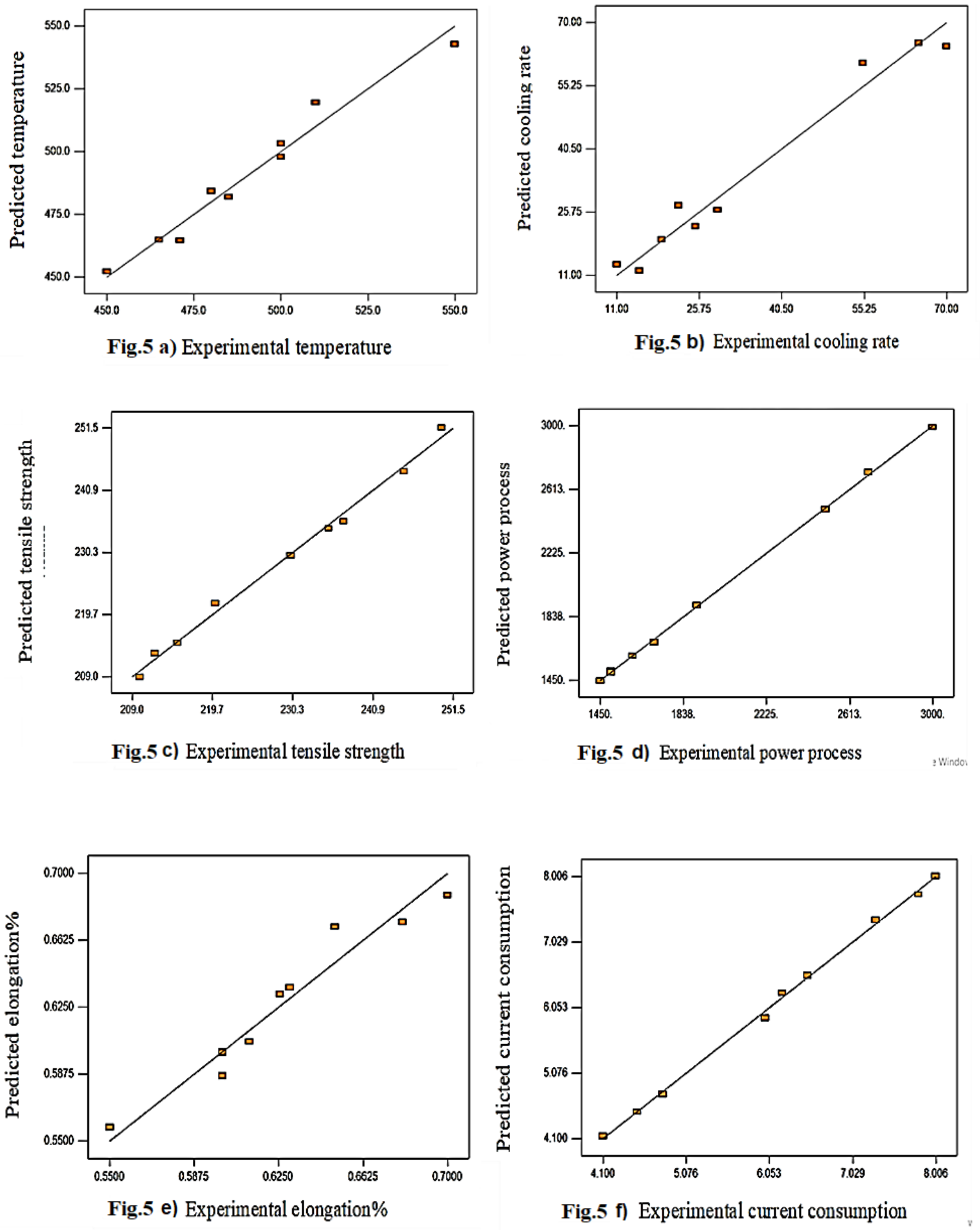

Figure5. Scatter diagram of predicted and experimental (a)temperature (b)cooling rate (c) tensile strength (d)power process (e)tensile strength (f) current consumption.

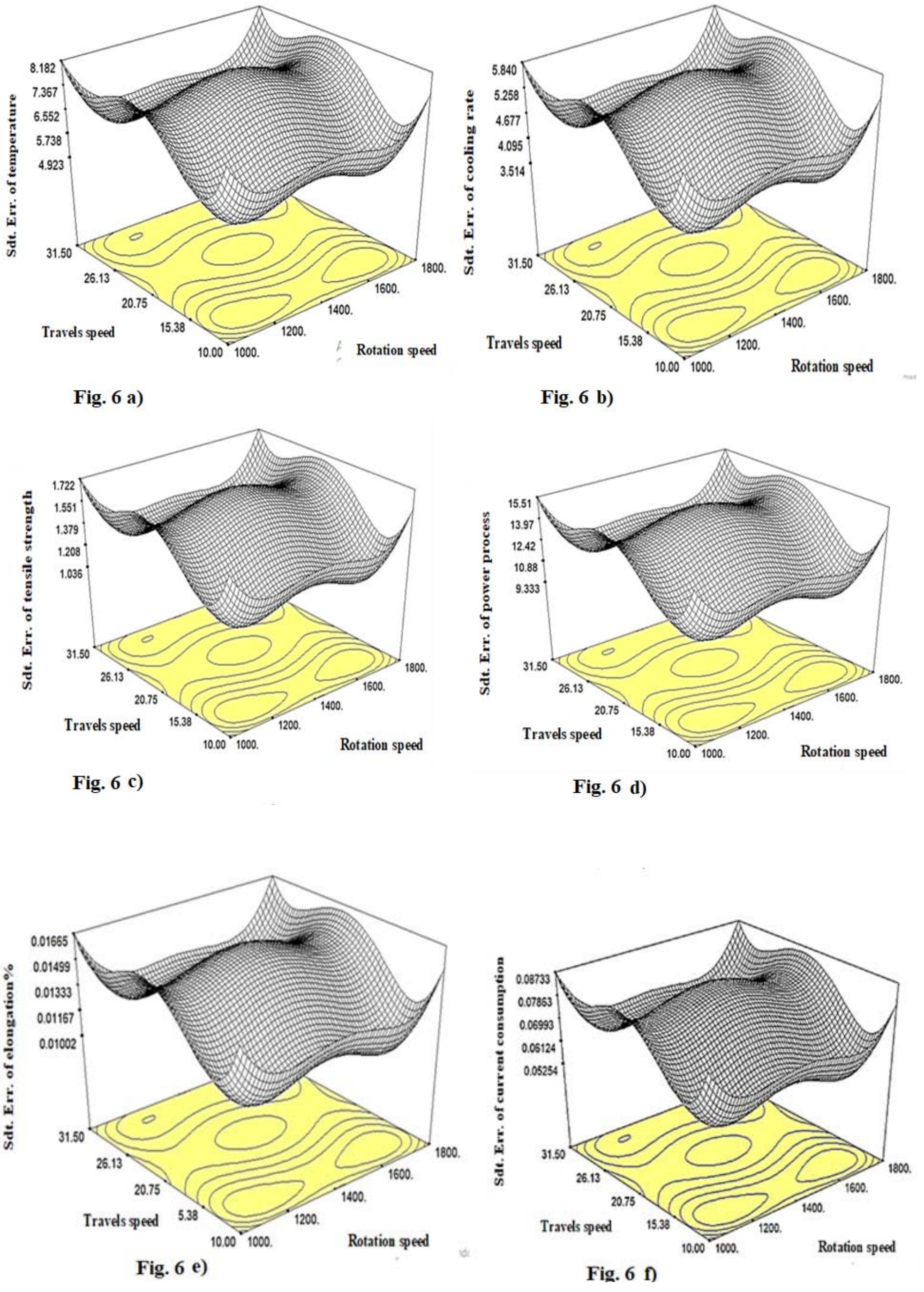

Figure6. Total stander error of predicted and experimental (a)temperature (b)cooling rate (c) tensile strength (d)power process (e)tensile strength (f) current consumption.

The heat production of FSW is related to the rotational speed and travels speed of the tool, yield shear stress, friction coefficient, contact pressure between the tool and the matrix, etc. the effect of different rotational speeds on the recorded welding thermal cycles. As the rotational speed increases from 1800 rpm to 1000 rpm, the peak temperature of the retreating side increases. When the speed reached 1800 rpm and travel speed 10 mm/min , the maximum temperature fell back to 550°C.For the aluminium

alloy, the tensile strength increases with increasing temperature, so the yield shear stress, contact pressure and friction coefficient will decrease with increasing temperature.
Therefore, when the rotational speed of the tool is increased and travels speed decrease, although the heat production may be increased and the temperature will rise, the yield shear stress, contact pressure and friction coefficient will decrease with increasing temperature, which will lead to a decrease in the actual heat production Because of this, FSW can keep the base metal in the solid state for welding.
The Rotational speed is directly proportional to the tensile strength of the weld. The frictional heat input increases with increase in the rotational rate of the tool. Thus the increase in the Rotational speed enhances the heat input of the process which in turn results in better material flow and increases the material to be displaced in a unit time. The maximum tensile strength, power and current consumption of the weld is also seen when the process parameter rotational speed set at a higher level in the process.
As travel speed is one of the important process parameters, the considered level doesn't affect the responses as the variation in the level average is not appreciable. This implies within the selected range of process window the levels can be fixed at any level to have the desired output show

3.4 Optimization of parameters of FSW
One of the most important aims of this investigation is to maximize tensile strength, elongation % and cooling rate and to minimize current consumption, power process, and temperature of FS welded joints of AA 6061 plate. From the mathematical model, the optimum process parameters are obtained with the desirability ranges between 0 and 1.The predicted optimal results from above technique are tensile strength, elongation percentage, current consumption, power, cooling rate and temperature that obtained using Design Expert software at the combined desirability value of 0.631.Figure7 shows the immediate influence of rotational speed on mechanical properties. It is seen that as the rotational speed increases the tensile strength, yield strength, hardness and percentage of elongation of Friction Stir welded aluminium alloy 6061 increases. In FSW as the rotational speed increases the heat input also increases and additional heat input destroys the regular flow behaviour. Figure 7 shows the immediate influence of travel speed on mechanical properties. It is evident that as traveling speed decreases from 31.5 to 10mm/min the mechanical properties of the FS welded AA 6061 increases and then decreases. At lowest traveling speed (10 mm/min) and highest traveling speed (31.5 mm/min) lower tensile strength is observed. This is due to the increased frictional heat and insufficient frictional heat generated respectively. Also higher traveling speed produce poor plasticflow of the material it causes poor consolidation of the metal interface.

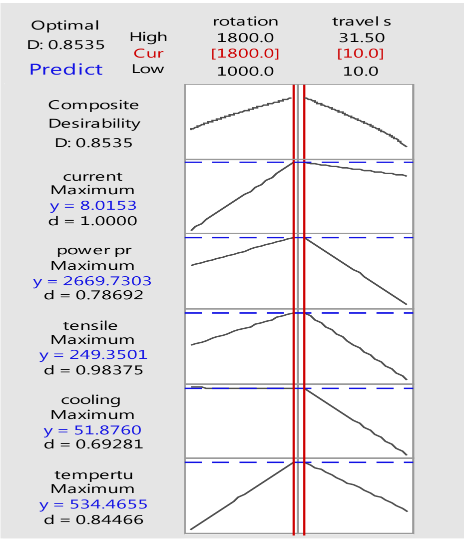

Figure7. Optimized parameters and responses using response optimizer in ANOVA

3.5 Analysis of results

The effects of the different process parameter on the mechanical properties of FS welded aluminium alloy 6061 are predicted from the mathematical models using the experimental observations are presented in figure 8 showing the general trends between cause and effect.In figure 9 shown contour Plot of current consumption, power process, tensile strength, cooling rate and temperature

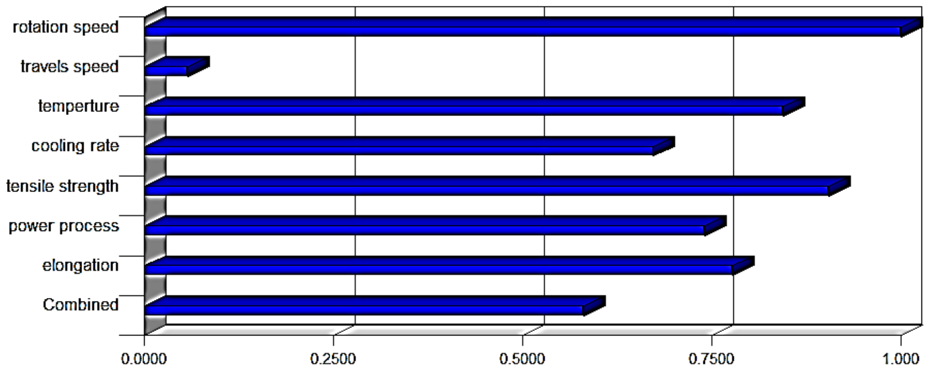

Figure8. Bar graph showing the maximum desirability for the combined desirability value of 0.631.

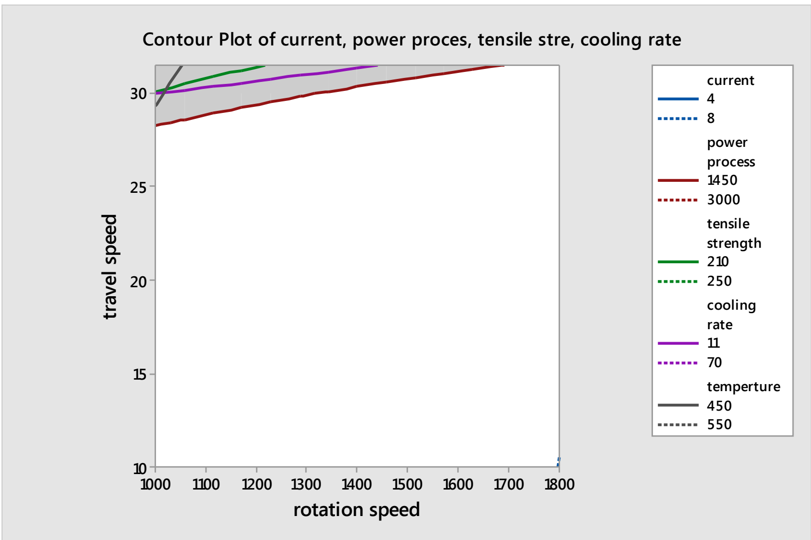

Figure9. Contour Plot of current consumption, power process, tensile strength, cooling rate and temperature.

4. Conclusions

In the present work, the minimum power and energy consumption of AA6061 butt welds created by friction stir welding were experimentally investigated over a wide range of spindle speeds from 100, 1400 and 1800 and travel speeds from 10, 16 and 31,5mm/min.

1- The consumed power is minimum with a combination of lowest spindle speed and high weld speed, while the current consumption is minimum by operating at the highest weld speed.
2- The consumed power increases with both increasing spindle speed and travel speed.
3- The results show that the measured temperature gradient at the tool-weld interface is an effective proxy for both the cooling rate trend and the resulting ultimate tensile strength.

References

[1] Mishra R Sand Ma Z Y 2005Friction stir welding and processing*Mater. Sci. Eng.R Report*s **50** pp 1–78.

[2] Fleming P, LammleinD, Wilkes D, Fleming K, Bloodworth T, Cook G, Strauss A, Lienert T and Bement M 2008 In-process gap detection in friction stir welding *Sens. Rev.* **28** pp 62–7.

[3] Arbegast W 2008A flow-partitioned deformation zone model for defect formation during friction stir welding*ScriptaMaterialia* **58** pp 372–6.

[4] Chen C, Kovacevic R and Jandgric D 2003 Wavelet transform analysis of acoustic emission in monitoring friction stir welding of 6061aluminum*Int. J. Mach. Tools Manuf.***43** pp 1383–90.

[5] SoundararajanV, Atharifar H and Kovacevic R 2006 Monitoring and processing the acoustic emission signals from the friction-stir-welding process*Proc. Inst. Mech. Eng. B J. Eng. Manuf.***220** pp 1673-85

[6] Upadhyay P and Reynolds A 2014 Effect of backing plate thermal property on friction stirwelding of 25-mm-thick AA6061*Metall. Mater. Trans.*A**45** pp 2091–100.

[7] Kumar U, Yadav I, Kumari S, Kumari K, Ranjan N, Kesharwani R, Jain R, Kumar S, Pal S, Chakravarty D and Pal S 2015 Defect identification in friction stir welding using discrete wavelet analysis*Adv. Eng. Softw.***85** pp 43–50.

[8] Das B, Pal Sand Bag S 2017 Weld quality prediction in friction stir welding usingwavelet analysis *Int. J. Adv. Manuf. Technol.***89** pp 711–25.

[9] Boldsaikhan E, Corwin E M, Logar A M and Arbegast W 2011 The use of neural network and discrete Fourier transform for real-time evaluation of friction stir welding *Appl. Soft Comput.***11** pp 4839–46.

[10] ShrivastavaA, Zinn M, Duffie N A, Ferrier N J, Smith, C B and Pfefferkorn F E 2017 Force measurement-based discontinuity detection during friction stir welding*J. Manuf. Process.***26** pp 113–21.

[11] El-Kassas A M and Sabry I 2019 A new quality monitoring system for friction stir welded joints of aluminumpipes *Int. J. Eng.Technol.* **11** pp 78–87.

[12] Shrivastava A, Krones M and Pfefferkorn F E 2015Comparison of energy consumption and environmental impact of friction stir welding and gas metal arc welding for aluminium *Proc. Inst. Mech. Eng. B J. Eng. Manuf.* **9** pp 159–68.

[13] Kumari S, Jain R, Kumar U, Yadav I, Ranjan N, Kumari K, Kesharwani R K, Kumar S, Pal S, Pal S K and Chakravarty D 2016 Defect identification in friction stir welding using continuous wavelet transform *J. Intell. Manuf.* **30** pp 483–94

[14] El-Kassas A M andSabry I 2019 Optimization of the underwater friction stir welding of pipes using hybrid RSM-fuzzy approach *Int.J. of Appl. Eng. Res.***14** pp 4562–72.